

RESEARCH ARTICLE



## Design, synthesis and biological evaluation of novel urolithin derivatives targeting liver cancer cells

Mi Tian<sup>a\*</sup>, Lirong Zhao<sup>b\*</sup>, Yu Lan<sup>c</sup>, Chen Li<sup>c</sup>, Yipeng Ling<sup>c</sup> and Benhong Zhou<sup>c</sup>

<sup>a</sup>Department of Pharmacy, The Central Hospital of Wuhan, Tongji Medical College, Huazhong University of Science and Technology, Wuhan, China;

<sup>b</sup>Department of Pharmacy, General Hospital of The Yangtze River Shipping, Wuhan, China; <sup>c</sup>Department of Pharmacy, Renmin Hospital of Wuhan University, Wuhan, China

### ABSTRACT

We designed and synthesised 22 new urolithin derivatives (UDs) based on methyl-urolithin A (mUA) to identify anti-cancer drugs with high efficacy and low toxicity and evaluated their anti-cancer activities *in vitro*. Cytotoxicity tests were performed on three cell lines (DU145, T24, and HepG2) and a human normal cell line (HK-2). The half-inhibitory concentration ( $IC_{50}$ ) of derivative UD-4c to hepatoma HepG2 cells ( $IC_{50} = 4.66 \pm 0.12 \mu M$ ) was significantly lower than that of sorafenib ( $IC_{50} = 7.76 \pm 0.12 \mu M$ ), and exhibited less toxicity to HK-2 cells. Preliminary studies on the mechanism revealed that the derivative UD-4c could significantly inhibit the HepG2 cell growth and colony formation, block the HepG2 cell cycle in the G2/M phase, and induce apoptosis of HepG2 cells dose-dependently. The derivative UD-4c can be used as a potential lead compound to further develop new drugs for hepatocellular carcinoma treatment based on the evaluation of anti-cancer activity.

### ARTICLE HISTORY

Received 12 January 2025

Revised 8 March 2025

Accepted 2 April 2025

### KEYWORDS

Urolithin derivatives; anti-cancer activity; hepatocellular carcinoma; proliferation; apoptosis; cell cycle

### Introduction

Cancer is becoming an urgent medical issue globally due to the annual increasing incidence and mortality rates<sup>1</sup>. It is imperative to develop new cancer treatment drugs.

Natural plants contain numerous natural active ingredients that are readily accessible and have good activity. Natural medicines or foods, including pomegranate, raspberry, and round-leaf grapes, are rich in ellagitannins, which have antioxidant<sup>2</sup>, antitumor<sup>3,4</sup>, antibacterial<sup>5</sup>, and antiviral properties<sup>6</sup>; however, they are poorly bioavailable in living organisms and are primarily metabolised by intestinal flora in the body to urolithins, which can accumulate in the body at concentrations of 0.2–20  $\mu M$ <sup>7</sup>. They are eventually excreted in the urine and faeces<sup>8,9</sup>. Urolithins are named urolithins A–D according to the number of hydroxyl groups and substitution positions<sup>10</sup>. Urolithins are uncommon and predominant in sulphated, glycosylated, and methylated forms. They are widely distributed in the urine, faeces, and bile of animals<sup>11,12</sup>.



Previous studies have reported that urolithin has various biological activities, including antioxidant<sup>13</sup>, anti-inflammatory<sup>14–16</sup>, neuroprotective<sup>17–19</sup>, and anti-cancer. The anti-cancer activity is one of the most extensively researched areas, and it has different degrees of anti-cancer effects on bladder<sup>20,21,24,25</sup>, lung<sup>22</sup>, liver<sup>23–25</sup>, colorectal<sup>26–29</sup>, prostate<sup>30–33</sup>, breast<sup>34–37</sup>, pancreatic ductal adenocarcinoma<sup>38</sup>, and endometrial cancer<sup>39–41</sup>. However, urolithin is a dibenzopyran-6-one derivative with a rigid skeletal structure, which results in poor water solubility and low bioavailability, and there is a need to improve its pharmacological activity, which

affects the drug-forming properties. Therefore, the structure was designed and modified herein to rectify the defective physico-chemical properties of urolithins. Based on the drug collocation principle, alkylation and amination reactions were used to synthesise a series of derivatives with the structure of mUA-spacer group-cyclic amine group, with mUA as the parent compound and cyclic amine group as the terminal structure and brominated alkanes as the flexible carbon chain connecting mUA and cyclic amine group. We screened the anti-cancer activity of the derivatives and preliminarily investigated the anti-cancer mechanism to obtain anti-cancer drugs with high anti-cancer activity, good solubility, high bioavailability, low toxic side effects, and new structures.

### Materials and methods

#### General remarks

All the chemical reagents and solvents were obtained from commercial companies (Wuhan Xinshenshi Chemical Technology Co., Ltd., Hubei, China) and were used without further purification. The <sup>1</sup>H NMR and <sup>13</sup>C NMR of all urolithin derivatives (UD-2a, UD-3a to UD-3g, UD-4a to UD-4g, UD-5a to UD-5g) were determined using Bruker NMR spectrometer (400, 101, and 151 MHz) with chemical shifts ( $\delta$  values) in parts per million of TMS units. Mass spectra were recorded using a high-resolution ESI on a Thermo Fisher Scientific ultra-high-resolution mass spectrometer at Wuhan University Medical Department. The purity was analytically determined using HPLC and was > 95%.

**CONTACT** Benhong Zhou  [benhongzh@whu.edu.cn](mailto:benhongzh@whu.edu.cn)  Department of Pharmacy, Renmin Hospital of Wuhan University, Wuhan 430060, China

\*These authors are co-first authors.

© 2025 The Author(s). Published by Informa UK Limited, trading as Taylor & Francis Group.

This is an Open Access article distributed under the terms of the Creative Commons Attribution-NonCommercial License (<http://creativecommons.org/licenses/by-nc/4.0/>), which permits unrestricted non-commercial use, distribution, and reproduction in any medium, provided the original work is properly cited. The terms on which this article has been published allow the posting of the Accepted Manuscript in a repository by the author(s) or with their consent.

HepG2(Catalogue number:SCSP-510), T24(Catalogue number:SCSP-536), DU145(Catalogue number:TCHu222), and HK-2(Catalogue number:SCSP-511) cells were procured from the Shanghai Cell Bank of the Chinese Academy of Sciences. HepG2 and HK-2 cells were cultured in DMEM medium, T24 cells in McCoys' 5A medium, and DU145 cells in MEM medium (containing NEAA). Unless otherwise stated, all media contained 10% foetal bovine serum, 1% 100U/mL penicillin, and 100mg/mL streptomycin. All cells were cultured in an incubator at 37°C with 5% CO<sub>2</sub>.

## Synthesis

### Synthesis of compound mUA

2-Bromo-5-methoxybenzoic acid (0.13mol, 30g), sodium hydroxide (0.28mol, 11.25g), and water (135ml) were added into a round bottom flask and stirred until the solution became clear. Resorcinol (0.27mol, 30g) was added and reacted for 90min in an oil bath at 70°C. Additionally, 5% of CuSO<sub>4</sub> (54ml) solution was added dropwise and reacted in an oil bath at 80°C. The reaction was monitored using TLC and completed after 2h. The reaction solution was subsequently washed with water and filtered, the solid was dried, the resulting solid was recrystallized with isopropanol, and the precipitated solid was filtered and dried again to obtain 12.2g of yellow-white solid powder.

**3-hydroxy-8-methoxy-6H-benzo[c]chromen-6-one(mUA).** Light yellow solid, yield 38.79%. <sup>1</sup>H NMR (400MHz, DMSO-*d*<sub>6</sub>) δ 10.22 (s, 1H), 8.18 (d, *J*=8.9Hz, 1H), 8.06 (d, *J*=8.7Hz, 1H), 7.58 (d, *J*=2.8Hz, 1H), 7.47 (dd, *J*=8.9, 2.8Hz, 1H), 6.81 (dd, *J*=8.7, 2.4Hz, 1H), 6.73 (d, *J*=2.4Hz, 1H), 3.88 (s, 3H). <sup>13</sup>C NMR (101MHz, DMSO-*d*<sub>6</sub>) δ 160.97, 159.40, 158.91, 151.60, 128.96, 124.57, 124.37, 123.98, 120.45, 113.53, 111.19, 109.94, 103.28, 55.99. U-HR-MS (ESI) *m/z*: Calcd. for C<sub>14</sub>H<sub>9</sub>O<sub>4</sub> [M-H]<sup>-</sup>: 241.0506. Found: 241.0505.

### Synthesis of compound UD-2a

Methyl urolithin A (2.06mmol, 500mg) and 4-(2-chloroethyl)morpholine hydrochloride (4.12mmol, 770mg) were added into a round-bottom flask. Subsequently, potassium carbonate (4.12mmol, 570mg) and acetone (60ml) were added. The reaction was stirred using a magnetic stirrer at 62°C in an oil bath. The reaction process was monitored using TLC and completed after 24h. Subsequently, the acetone was evaporated using a rotary evaporator, and the sample was purified with dichloromethane and silica gel, followed by silica gel column chromatography to separate the target product. The eluate containing the target product was evaporated using a rotary evaporator with a gradient elution with petroleum ether and ethyl acetate as the mobile phases, and 644.8mg of white solid powder was obtained.

**8-methoxy-3-(2-morpholinoethoxy)-6H-benzo[c]chromen-6-one(UD-2a).** White solid, yield 87.90%. <sup>1</sup>H NMR (400MHz, DMSO-*d*<sub>6</sub>) δ 8.25 (d, *J*=9.0Hz, 1H), 8.16 (d, *J*=8.7Hz, 1H), 7.60 (d, *J*=2.8Hz, 1H), 7.50 (dd, *J*=8.8, 2.8Hz, 1H), 7.08–6.93 (*m*, 2H), 4.19 (*t*, *J*=5.7Hz, 2H), 3.90 (*s*, 3H), 3.60 (*t*, *J*=4.6Hz, 4H), 3.35 (*s*, 2H), 2.62 (d, *J*=85.6Hz, 4H). <sup>13</sup>C NMR (151MHz, DMSO-*d*<sub>6</sub>) δ 160.42, 159.57, 158.84, 151.09, 128.13, 124.08, 123.94, 123.92, 120.39, 112.72, 110.93, 110.83, 101.98, 66.12, 65.83, 56.83, 55.62, 53.56. U-HR-MS (ESI) *m/z*: Calcd. for C<sub>20</sub>H<sub>22</sub>NO<sub>5</sub> [M+H]<sup>+</sup>: 356.1492. Found: 356.1485.

### Synthesis of compound UD-3a~UD-3g

Methyl urolithin A (82.57mmol, 20g), 1,3-dibromopropane (165.14mmol, 33.4g), potassium carbonate (165.14mmol, 22.8g), and acetone (240ml) were added into a round-bottom flask, and

the reaction was stirred at 62°C in an oil bath. The reaction was monitored using TLC and completed after 24h. The reaction was subsequently evaporated using a rotary evaporator. The acetone was extracted, and dichloromethane and silica gel were added to purify the sample. Subsequently, silica gel column chromatography was used to separate the target product, and the eluate containing the target product was evaporated using a rotary evaporator with petroleum ether and ethyl acetate as the mobile phase gradient to obtain 5.95g of urolithin intermediate (UI) UI-1

UI-1 (0.55mmol, 200mg), potassium carbonate (cyclic amine group: 1.1mmol, 152mg; open chain amine group: 1.65mmol, 228mg), acetonitrile (30ml), and a small amount of potassium iodide were added into a round bottom flask. Subsequently, the amine group was added to the reaction at a molar ratio of UI-1: cyclic amine group terminal of 1:1.1. The reaction was performed in an oil bath at 82°C. The reaction was monitored using TLC and the iodine cylinder colour development principle, and the process was completed after 24h. The acetonitrile was subsequently evaporated using a rotary evaporator. Dichloromethane and silica gel were added to purify the sample. The sample was subjected to silica gel column chromatography to separate the target product. The eluate containing the target product was evaporated using a rotary evaporator with petroleum ether and ethyl acetate or dichloromethane and methanol as the mobile phase gradient. The resulting solid was dissolved in dichloromethane and filtered. The resulting solid was dissolved in dichloromethane and filtered, and the filtrate was evaporated and dried to obtain the derivatives UD-3a~UD-3g.

**3-(3-bromopropoxy)-8-methoxy-6H-benzo[c]chromen-6-one(UI-1).** White solid, yield 19.84%. <sup>1</sup>H NMR (400MHz, DMSO-*d*<sub>6</sub>) δ 8.26 (d, *J*=8.9Hz, 1H), 8.18 (d, *J*=8.5Hz, 1H), 7.61 (d, *J*=2.8Hz, 1H), 7.50 (dd, *J*=8.9, 2.8Hz, 1H), 7.01 (*s*, 2H), 6.99 (d, *J*=2.6Hz, 1H), 4.19 (*t*, *J*=5.9Hz, 2H), 3.90 (*s*, 3H), 3.70 (*t*, *J*=6.5Hz, 2H), 2.29 (*p*, *J*=6.3Hz, 2H). <sup>13</sup>C NMR (101MHz, DMSO-*d*<sub>6</sub>) δ 160.88, 159.89, 159.31, 151.54, 128.55, 124.64, 124.42, 120.88, 113.06, 111.45, 111.35, 102.45, 66.34, 56.09, 32.14, 31.62. U-HR-MS (ESI) *m/z*: Calcd. for C<sub>17</sub>H<sub>16</sub>BrO<sub>4</sub> [M+H]<sup>+</sup>: 363.0226. Found: 363.0226.

**8-methoxy-3-(3-(pyrrolidin-1-yl)propoxy)-6H-benzo[c]chromen-6-one(UD-3a).** Yellow-white solid, yield 72.92%. <sup>1</sup>H NMR (400MHz, DMSO-*d*<sub>6</sub>) δ 8.27 (d, *J*=9.0Hz, 1H), 8.22–8.14 (*m*, 1H), 7.61 (d, *J*=2.8Hz, 1H), 7.51 (dd, *J*=8.9, 2.9Hz, 1H), 7.05–6.92 (*m*, 2H), 4.14 (*t*, *J*=6.2Hz, 2H), 3.90 (*s*, 3H), 2.83 (d, *J*=23.2Hz, 6H), 2.01 (*p*, *J*=6.4Hz, 2H), 1.80 (*p*, *J*=3.3Hz, 4H). <sup>13</sup>C NMR (101MHz, DMSO-*d*<sub>6</sub>) δ 160.87, 160.02, 159.27, 151.52, 128.55, 124.57, 124.40, 124.37, 120.81, 113.04, 111.33, 111.28, 102.34, 66.48, 56.08, 54.02, 52.30, 27.48, 23.38. U-HR-MS (ESI) *m/z*: Calcd. for C<sub>21</sub>H<sub>24</sub>NO<sub>4</sub> [M+H]<sup>+</sup>: 354.1700. Found: 354.1700.

**8-methoxy-3-(3-(piperidin-1-yl)propoxy)-6H-benzo[c]chromen-6-one(UD-3b).** Yellow-white solid, yield 62.45%. <sup>1</sup>H NMR (400MHz, Chloroform-*d*) δ 7.91 (d, *J*=8.9Hz, 1H), 7.85 (d, *J*=8.8Hz, 1H), 7.76 (d, *J*=2.8Hz, 1H), 7.36 (dd, *J*=8.8, 2.8Hz, 1H), 6.90 (dd, *J*=8.8, 2.6Hz, 1H), 6.86 (d, *J*=2.5Hz, 1H), 4.07 (*t*, *J*=6.3Hz, 2H), 3.92 (*s*, 3H), 2.50 (dd, *J*=8.4, 6.6Hz, 2H), 2.42 (*s*, 4H), 2.08–1.96 (*m*, 2H), 1.60 (*q*, *J*=5.6Hz, 4H), 1.46 (d, *J*=6.9Hz, 2H). <sup>13</sup>C NMR (151MHz, Chloroform-*d*) δ 161.83, 160.37, 159.34, 151.84, 128.94, 124.65, 123.27, 122.99, 121.18, 112.95, 111.40, 111.20, 102.42, 67.16, 56.02, 55.94, 54.85, 26.81, 26.10, 24.57. U-HR-MS (ESI) *m/z*: Calcd. for C<sub>22</sub>H<sub>26</sub>NO<sub>4</sub> [M+H]<sup>+</sup>: 368.1856. Found: 368.1856.

**3-(3-(Azepan-1-yl)propoxy)-8-methoxy-6H-benzo[c]chromen-6-one(UD-3c).** Yellow-white solid, yield 62.95%. <sup>1</sup>H NMR (400MHz, Chloroform-*d*) δ 7.92 (d, *J*=8.9Hz, 1H), 7.85 (d, *J*=8.8Hz, 1H), 7.76

(d,  $J=2.8$  Hz, 1H), 7.37 (dd,  $J=8.8$ , 2.8 Hz, 1H), 6.90 (dd,  $J=8.7$ , 2.5 Hz, 1H), 6.86 (d,  $J=2.5$  Hz, 1H), 4.08 (t,  $J=6.3$  Hz, 2H), 3.93 (s, 3H), 2.69 (td,  $J=6.4$ , 5.8, 3.0 Hz, 6H), 2.06–1.95 (m, 2H), 1.72–1.57 (m, 8H).  $^{13}\text{C}$  NMR (151 MHz, Chloroform- $d$ )  $\delta$  161.86, 160.42, 159.35, 151.86, 128.96, 124.67, 123.28, 123.00, 121.19, 112.97, 111.40, 111.21, 102.43, 67.04, 55.96, 55.71, 54.78, 28.09, 27.46, 27.22. U-HR-MS (ESI)  $m/z$ : Calcd. for  $\text{C}_{23}\text{H}_{28}\text{NO}_4$   $[\text{M}+\text{H}]^+$ : 382.2013. Found: 382.2013.

**8-methoxy-3-(3-(4-methylpiperidin-1-yl)propoxy)-6H-benzo[*c*]chromen-6-one(UD-3d).** Yellow solid, yield 51.75%.  $^1\text{H}$  NMR (400 MHz, Chloroform- $d$ )  $\delta$  7.92 (d,  $J=8.9$  Hz, 1H), 7.85 (d,  $J=8.8$  Hz, 1H), 7.76 (d,  $J=2.8$  Hz, 1H), 7.37 (dd,  $J=8.8$ , 2.8 Hz, 1H), 6.89 (dd,  $J=8.8$ , 2.5 Hz, 1H), 6.84 (d,  $J=2.5$  Hz, 1H), 4.09 (t,  $J=6.2$  Hz, 2H), 3.93 (s, 3H), 3.08 (d,  $J=10.7$  Hz, 2H), 2.73–2.64 (m, 2H), 2.21–2.09 (m, 4H), 1.72 (s, 1H), 1.49–1.37 (m, 4H), 0.96 (d,  $J=5.5$  Hz, 3H).  $^{13}\text{C}$  NMR (101 MHz, Chloroform- $d$ )  $\delta$  161.60, 159.90, 159.13, 151.54, 128.62, 124.44, 123.13, 122.81, 120.93, 112.55, 111.30, 110.94, 102.24, 66.63, 55.77, 55.38, 53.87, 33.46, 30.42, 26.20, 21.68. U-HR-MS (ESI)  $m/z$ : Calcd. for  $\text{C}_{23}\text{H}_{28}\text{NO}_4$   $[\text{M}+\text{H}]^+$ : 382.2013. Found: 382.2013.

**8-methoxy-3-(3-morpholinopropoxy)-6H-benzo[*c*]chromen-6-one(UD-3e).** White solid, yield 79.17%.  $^1\text{H}$  NMR (400 MHz, Chloroform- $d$ )  $\delta$  7.92 (d,  $J=8.9$  Hz, 1H), 7.85 (d,  $J=8.7$  Hz, 1H), 7.76 (d,  $J=2.8$  Hz, 1H), 7.37 (dd,  $J=8.8$ , 2.8 Hz, 1H), 6.90 (dd,  $J=8.8$ , 2.6 Hz, 1H), 6.86 (d,  $J=2.5$  Hz, 1H), 4.09 (t,  $J=6.3$  Hz, 2H), 3.93 (s, 3H), 3.74 (t,  $J=4.7$  Hz, 4H), 2.55 (t,  $J=7.3$  Hz, 2H), 2.49 (t,  $J=4.7$  Hz, 4H), 2.01 (p,  $J=6.6$  Hz, 2H).  $^{13}\text{C}$  NMR (101 MHz, Chloroform- $d$ )  $\delta$  161.60, 160.04, 159.11, 151.58, 128.64, 124.45, 123.10, 122.78, 120.92, 112.72, 111.22, 110.93, 102.10, 66.99, 66.55, 55.74, 55.41, 53.76, 26.27. U-HR-MS (ESI)  $m/z$ : Calcd. for  $\text{C}_{21}\text{H}_{24}\text{NO}_5$   $[\text{M}+\text{H}]^+$ : 370.1649. Found: 370.1649.

**8-methoxy-3-(3-(4-methylpiperazin-1-yl)propoxy)-6H-benzo[*c*]chromen-6-one(UD-3f).** Yellow-white solid, yield 66.29%.  $^1\text{H}$  NMR (400 MHz, DMSO- $d_6$ )  $\delta$  8.27 (d,  $J=9.0$  Hz, 1H), 8.22–8.15 (m, 1H), 7.62 (d,  $J=2.8$  Hz, 1H), 7.52 (dd,  $J=8.9$ , 2.8 Hz, 1H), 6.98 (d,  $J=7.5$  Hz, 2H), 4.12 (t,  $J=6.3$  Hz, 2H), 3.91 (s, 3H), 2.64 (d,  $J=69.9$  Hz, 10H), 2.44 (s, 3H), 1.93 (p,  $J=6.5$  Hz, 2H).  $^{13}\text{C}$  NMR (101 MHz, DMSO- $d_6$ )  $\delta$  160.90, 160.14, 159.28, 151.55, 128.59, 124.59, 124.44, 124.40, 120.82, 113.09, 111.35, 111.24, 102.31, 66.69, 56.09, 54.20, 53.92, 51.50, 26.20. U-HR-MS (ESI)  $m/z$ : Calcd. for  $\text{C}_{22}\text{H}_{27}\text{N}_2\text{O}_4$   $[\text{M}+\text{H}]^+$ : 383.1965. Found: 383.1960.

**8-methoxy-3-(3-(4-phenylpiperazin-1-yl)propoxy)-6H-benzo[*c*]chromen-6-one(UD-3g).** White solid, yield 44.81%.  $^1\text{H}$  NMR (400 MHz, Chloroform- $d$ )  $\delta$  7.92 (d,  $J=8.9$  Hz, 1H), 7.86 (d,  $J=8.8$  Hz, 1H), 7.77 (d,  $J=2.8$  Hz, 1H), 7.37 (dd,  $J=8.8$ , 2.8 Hz, 1H), 7.32–7.23 (m, 2H), 6.99–6.82 (m, 5H), 4.11 (t,  $J=6.3$  Hz, 2H), 3.93 (s, 3H), 3.28–3.21 (m, 4H), 2.67 (t,  $J=5.0$  Hz, 4H), 2.63 (t,  $J=7.3$  Hz, 2H), 2.07 (p,  $J=6.6$  Hz, 2H).  $^{13}\text{C}$  NMR (101 MHz, Chloroform- $d$ )  $\delta$  161.63, 160.08, 159.14, 151.62, 151.29, 129.14, 128.68, 124.49, 123.13, 122.82, 120.96, 119.75, 116.09, 112.73, 111.26, 110.95, 102.17, 66.67, 55.77, 55.07, 53.32, 49.14, 26.60. U-HR-MS (ESI)  $m/z$ : Calcd. for  $\text{C}_{27}\text{H}_{29}\text{N}_2\text{O}_4$   $[\text{M}+\text{H}]^+$ : 445.2122. Found: 445.2121.

#### Synthesis of compound UD-4a~UD-4g

Methyl urolithin A (82.57 mmol, 20 g), 1,4-dibromobutane (165.14 mmol, 35.7 g), potassium carbonate (165.14 mmol, 22.8 g), and acetone (240 ml) were added into a round-bottom flask. The reaction was stirred at 62°C in an oil bath. The reaction process was monitored using TLC and completed after 24 h. The acetone was removed by evaporation using a rotary evaporator. Dichloromethane and silica gel

were added to purify the sample, followed by silica gel column chromatography to separate the target product. The eluate containing the target product was evaporated using a rotary evaporator with petroleum ether and ethyl acetate as mobile phases in gradient elution to obtain 5.48 g of intermediate UI-2.

UI-2 (0.53 mmol, 200 mg), potassium carbonate (cyclic amine group: 1.06 mmol, 147 mg; open chain amine group: 1.59 mmol, 220 mg), acetonitrile (30 ml), and a small amount of potassium iodide were added into a round bottom flask. Subsequently, the amine group terminals were added to the reaction at a molar ratio of UI-2: cyclic amine group terminal of 1:1.1. The reaction was magnetically stirred in an oil bath at 82°C. The reaction was monitored using TLC and the iodine cylinder colour development principle, and the process was completed after 24 h. Subsequently, the acetonitrile was removed by evaporation using a rotary evaporator, and dichloromethane and silica gel were added to purify the sample, followed by silica gel column chromatography to separate the target product. The eluate containing the target product was evaporated using a rotary evaporator with petroleum ether and ethyl acetate or dichloromethane and methanol as the mobile phase gradient. The resulting solid was dissolved in dichloromethane and filtered, and the filtrate was evaporated and dried to obtain the derivatives UD-4a~UD-4g.

**3-(4-bromobutoxy)-8-methoxy-6H-benzo[*c*]chromen-6-one(UI-2).** White solid, yield 17.59%.  $^1\text{H}$  NMR (400 MHz, DMSO- $d_6$ )  $\delta$  8.24 (d,  $J=9.0$  Hz, 1H), 8.18–8.11 (m, 1H), 7.59 (d,  $J=2.8$  Hz, 1H), 7.49 (dd,  $J=8.9$ , 2.9 Hz, 1H), 6.96 (d,  $J=7.9$  Hz, 2H), 4.09 (t,  $J=6.3$  Hz, 2H), 3.89 (s, 3H), 3.63 (t,  $J=6.6$  Hz, 2H), 2.04–1.91 (m, 2H), 1.94–1.78 (m, 2H).  $^{13}\text{C}$  NMR (101 MHz, DMSO- $d_6$ )  $\delta$  160.87, 160.08, 159.23, 151.52, 128.57, 124.51, 124.36, 124.33, 120.78, 113.05, 111.29, 111.20, 102.27, 67.65, 56.06, 35.30, 29.48, 27.70. U-HR-MS (ESI)  $m/z$ : Calcd. for  $\text{C}_{18}\text{H}_{18}\text{BrO}_4$   $[\text{M}+\text{H}]^+$ : 377.0383. Found: 377.0383.

**8-methoxy-3-(4-(pyrrolidin-1-yl)butoxy)-6H-benzo[*c*]chromen-6-one(UD-4a).** Yellow solid, yield 91.37%.  $^1\text{H}$  NMR (400 MHz, DMSO- $d_6$ )  $\delta$  8.28 (d,  $J=8.9$  Hz, 1H), 8.20 (d,  $J=8.6$  Hz, 1H), 7.62 (d,  $J=2.8$  Hz, 1H), 7.52 (dd,  $J=8.9$ , 2.9 Hz, 1H), 7.04–6.96 (m, 2H), 4.13 (d,  $J=5.6$  Hz, 2H), 3.91 (s, 3H), 3.22 (t,  $J=7.5$  Hz, 2H), 3.21 (s, 2H), 2.02–1.77 (m, 10H).  $^{13}\text{C}$  NMR (151 MHz, DMSO- $d_6$ )  $\delta$  160.42, 159.59, 158.88, 151.11, 128.12, 124.16, 123.99, 123.97, 120.40, 112.66, 110.97, 110.88, 101.97, 67.39, 55.65, 53.66, 53.21, 40.05, 25.60, 22.59, 22.20. U-HR-MS (ESI)  $m/z$ : Calcd. for  $\text{C}_{22}\text{H}_{26}\text{NO}_4$   $[\text{M}+\text{H}]^+$ : 368.1856. Found: 368.1851.

**8-methoxy-3-(4-(piperidin-1-yl)butoxy)-6H-benzo[*c*]chromen-6-one(UD-4b).** Yellow-white solid, yield 77.13%.  $^1\text{H}$  NMR (400 MHz, DMSO- $d_6$ )  $\delta$  8.28 (d,  $J=9.0$  Hz, 1H), 8.19 (d,  $J=8.7$  Hz, 1H), 7.62 (d,  $J=2.8$  Hz, 1H), 7.52 (dd,  $J=8.9$ , 2.8 Hz, 1H), 7.03–6.95 (m, 2H), 4.14–4.07 (m, 2H), 3.90 (s, 3H), 2.85 (s, 6H), 1.88–1.40 (m, 10H).  $^{13}\text{C}$  NMR (101 MHz, DMSO- $d_6$ )  $\delta$  160.89, 160.08, 159.27, 151.54, 128.57, 124.57, 124.39, 120.80, 113.08, 111.33, 111.24, 102.32, 68.03, 56.79, 56.07, 53.16, 26.41, 23.99, 22.71, 21.53. U-HR-MS (ESI)  $m/z$ : Calcd. for  $\text{C}_{23}\text{H}_{28}\text{NO}_4$   $[\text{M}+\text{H}]^+$ : 382.2013. Found: 382.2007.

**3-(4-(Azepan-1-yl)butoxy)-8-methoxy-6H-benzo[*c*]chromen-6-one(UD-4c).** Yellow solid, yield 50.07%.  $^1\text{H}$  NMR (400 MHz, DMSO- $d_6$ )  $\delta$  8.27 (d,  $J=9.0$  Hz, 1H), 8.22–8.14 (m, 1H), 7.61 (d,  $J=2.8$  Hz, 1H), 7.51 (dd,  $J=8.9$ , 2.9 Hz, 1H), 6.98 (d,  $J=8.1$  Hz, 2H), 4.09 (t,  $J=6.3$  Hz, 2H), 3.90 (s, 3H), 2.76 (d,  $J=35.0$  Hz, 6H), 1.86–1.50 (m, 12H).  $^{13}\text{C}$  NMR (101 MHz, DMSO- $d_6$ )  $\delta$  160.88, 160.16, 159.23, 151.53, 128.59, 124.52, 124.38, 124.33, 120.77, 113.06, 111.30, 111.14, 102.24, 68.28, 57.22, 56.07, 54.94, 26.80, 26.63, 23.25. U-HR-MS (ESI)  $m/z$ : Calcd. for  $\text{C}_{24}\text{H}_{30}\text{NO}_4$   $[\text{M}+\text{H}]^+$ : 396.2169. Found: 396.2170.



**8-methoxy-3-(4-(4-methylpiperidin-1-yl)butoxy)-6H-benzo[c]chromen-6-one(UD-4d).** Yellow-white solid, yield 70.72%. <sup>1</sup>H NMR (400 MHz, Chloroform-*d*) δ 7.92 (d, *J*=8.9 Hz, 1H), 7.85 (d, *J*=8.8 Hz, 1H), 7.76 (d, *J*=2.7 Hz, 1H), 7.37 (dd, *J*=8.8, 2.8 Hz, 1H), 6.92–6.82 (m, 2H), 4.03 (t, *J*=6.3 Hz, 2H), 3.93 (s, 3H), 2.93 (d, *J*=10.4 Hz, 2H), 2.44–2.36 (m, 2H), 1.99–1.78 (m, 5H), 1.77–1.60 (m, 4H), 1.27 (qd, *J*=11.9, 3.6 Hz, 2H), 0.93 (d, *J*=6.1 Hz, 3H). <sup>13</sup>C NMR (101 MHz, Chloroform-*d*) δ 161.65, 160.14, 159.08, 151.60, 128.72, 124.46, 123.07, 122.78, 120.90, 112.77, 111.11, 110.91, 102.04, 68.23, 58.66, 55.74, 54.08, 34.32, 30.85, 27.25, 23.61, 21.94. U-HR-MS (ESI) *m/z*: Calcd. for C<sub>24</sub>H<sub>30</sub>NO<sub>4</sub> [M+H]<sup>+</sup>: 396.2169. Found: 396.2164.

**8-methoxy-3-(4-morpholinobutoxy)-6H-benzo[c]chromen-6-one(UD-4e).** Light yellow solid, yield 84.12%. <sup>1</sup>H NMR (400 MHz, Chloroform-*d*) δ 7.92 (d, *J*=8.9 Hz, 1H), 7.86 (d, *J*=8.8 Hz, 1H), 7.76 (d, *J*=2.8 Hz, 1H), 7.37 (dd, *J*=8.8, 2.8 Hz, 1H), 6.89 (dd, *J*=8.7, 2.5 Hz, 1H), 6.85 (d, *J*=2.5 Hz, 1H), 4.05 (t, *J*=6.3 Hz, 2H), 3.93 (s, 3H), 3.73 (t, *J*=4.7 Hz, 4H), 2.48 (s, 4H), 2.46–2.39 (m, 2H), 1.86 (dt, *J*=8.6, 6.4 Hz, 2H), 1.71 (ddd, *J*=14.8, 9.0, 6.1 Hz, 2H). <sup>13</sup>C NMR (101 MHz, Chloroform-*d*) δ 161.63, 160.07, 159.11, 151.60, 128.68, 124.48, 123.11, 122.79, 120.92, 112.75, 111.18, 110.93, 102.02, 68.11, 66.98, 58.58, 55.75, 53.72, 27.02, 23.05. U-HR-MS (ESI) *m/z*: Calcd. for C<sub>22</sub>H<sub>26</sub>NO<sub>5</sub> [M+H]<sup>+</sup>: 384.1805. Found: 384.1802.

**8-methoxy-3-(4-(4-methylpiperazin-1-yl)butoxy)-6H-benzo[c]chromen-6-one(UD-4f).** White solid, yield 90.39%. <sup>1</sup>H NMR (400 MHz, DMSO-*d*<sub>6</sub>) δ 8.27 (d, *J*=9.0 Hz, 1H), 8.18 (d, *J*=8.8 Hz, 1H), 7.62 (d, *J*=2.8 Hz, 1H), 7.52 (dd, *J*=8.9, 2.9 Hz, 1H), 7.04–6.94 (m, 2H), 4.09 (t, *J*=6.3 Hz, 2H), 3.90 (s, 3H), 3.78–2.63 (m, 10H), 2.57 (s, 3H), 1.77 (p, *J*=6.4 Hz, 2H), 1.64 (d, *J*=12.5 Hz, 2H). <sup>13</sup>C NMR (101 MHz, Chloroform-*d*) δ 161.63, 160.07, 159.11, 151.60, 128.68, 124.48, 123.11, 122.79, 120.92, 112.75, 111.18, 110.93, 102.02, 68.11, 66.98, 58.58, 55.75, 53.72, 27.02, 23.05. U-HR-MS (ESI) *m/z*: Calcd. for C<sub>23</sub>H<sub>29</sub>N<sub>2</sub>O<sub>4</sub> [M+H]<sup>+</sup>: 397.2122. Found: 397.2128.

**8-methoxy-3-(4-(4-phenylpiperazin-1-yl)butoxy)-6H-benzo[c]chromen-6-one(UD-4g).** White solid, yield 81.03%. <sup>1</sup>H NMR (400 MHz, Chloroform-*d*) δ 7.92 (d, *J*=8.9 Hz, 1H), 7.86 (d, *J*=8.8 Hz, 1H), 7.77 (d, *J*=2.8 Hz, 1H), 7.37 (dd, *J*=8.8, 2.8 Hz, 1H), 7.27 (d, *J*=15.8 Hz, 1H), 6.97–6.81 (m, 6H), 4.06 (t, *J*=6.2 Hz, 2H), 3.93 (s, 3H), 3.22 (t, *J*=5.0 Hz, 4H), 2.68–2.61 (m, 4H), 2.54–2.45 (m, 2H), 1.94–1.83 (m, 2H), 1.81–1.69 (m, 2H). <sup>13</sup>C NMR (101 MHz, Chloroform-*d*) δ 161.65, 160.11, 159.12, 151.62, 151.32, 129.13, 128.70, 124.49, 123.13, 122.81, 120.94, 119.71, 116.05, 112.78, 111.19, 110.94, 102.06, 68.17, 58.22, 55.76, 53.29, 49.15, 27.13, 23.43. U-HR-MS (ESI) *m/z*: Calcd. for C<sub>28</sub>H<sub>31</sub>N<sub>2</sub>O<sub>4</sub> [M+H]<sup>+</sup>: 459.2278. Found: 459.2276.

#### Synthesis of compound UD-5a~UD-5g

Methyl urushiol A (82.57 mmol, 20 g), 1,5-dibromobutane (165.14 mmol, 38 g), potassium carbonate (165.14 mmol, 22.8 g), and acetone (240 ml) were added into a round-bottom flask. The reaction was stirred in an oil bath at 62 °C. The reaction was monitored using TLC and completed after 24 h. The acetone was evaporated using a rotary evaporator. Subsequently, the sample was purified with dichloromethane and silica gel, followed by silica gel column chromatography to separate the target product. The eluate containing the target product was evaporated using a rotary evaporator to obtain 5.79 g of intermediate UI-3.

UI-3 (0.51 mmol, 200 mg), potassium carbonate (cyclic amine group: 1.02 mmol, 141 mg; open chain amine group: 1.53 mmol, 212 mg), acetonitrile (30 ml), and a small amount of potassium iodide were added into a round bottom flask, and the amine

group terminals were added into the reaction at a molar ratio of UI-3:amine group terminals of 1:1.1. The oil bath was stirred magnetically at 82 °C, and the reaction was monitored using TLC and the iodine cylinder colour development principle and completed after 24 h. Subsequently, the acetonitrile evaporated using a rotary evaporator. Subsequently, dichloromethane and silica gel were added to purify the sample, followed by silica gel column chromatography to separate the target product. The eluate containing the target product was evaporated using a rotary evaporator with petroleum ether and ethyl acetate or dichloromethane and methanol as the mobile phase gradient. The resulting solid was dissolved with dichloromethane and filtered, and the filtrate was evaporated and dried to obtain the derivatives UD-5a~UD-5g.

**3-((5-bromopentyl)oxy)-8-methoxy-6H-benzo[c]chromen-6-one(Intermediate3).** White solid, yield 17.92%. <sup>1</sup>H NMR (400 MHz, DMSO-*d*<sub>6</sub>) δ 8.23 (d, *J*=9.0 Hz, 1H), 8.14 (d, *J*=9.6 Hz, 1H), 7.59 (d, *J*=2.8 Hz, 1H), 7.48 (dd, *J*=8.8, 2.8 Hz, 1H), 6.99–6.91 (m, 2H), 4.05 (t, *J*=6.4 Hz, 2H), 3.88 (s, 3H), 3.57 (t, *J*=6.7 Hz, 2H), 1.88 (dt, *J*=14.6, 6.8 Hz, 2H), 1.76 (p, *J*=6.6 Hz, 2H), 1.61–1.45 (m, 2H). <sup>13</sup>C NMR (101 MHz, DMSO-*d*<sub>6</sub>) δ 160.86, 160.24, 160.16, 159.19, 151.51, 128.57, 124.47, 124.33, 124.29, 120.75, 113.02, 111.27, 111.12, 102.21, 68.33, 56.02, 35.54, 32.41, 28.13, 24.72. U-HR-MS (ESI) *m/z*: Calcd. for C<sub>19</sub>H<sub>20</sub>BrO<sub>4</sub> [M+H]<sup>+</sup>: 391.0539. Found: 391.0539.

**8-methoxy-3-((5-(pyrrolidin-1-yl)pentyl)oxy)-6H-benzo[c]chromen-6-one(UD-5a).** White solid, yield 67.03%. <sup>1</sup>H NMR (400 MHz, DMSO-*d*<sub>6</sub>) δ 8.27 (d, *J*=9.0 Hz, 1H), 8.21–8.14 (m, 1H), 7.61 (d, *J*=2.8 Hz, 1H), 7.51 (dd, *J*=8.9, 2.9 Hz, 1H), 6.98 (d, *J*=8.2 Hz, 2H), 4.08 (t, *J*=6.4 Hz, 2H), 3.90 (s, 3H), 2.95 (s, 4H), 2.87 (t, *J*=7.8 Hz, 2H), 1.84 (p, 4H), 1.77 (q, *J*=7.0 Hz, 2H), 1.63 (p, *J*=15.4, 7.6 Hz, 2H), 1.53–1.40 (m, 2H). <sup>13</sup>C NMR (101 MHz, DMSO-*d*<sub>6</sub>) δ 160.90, 160.19, 159.26, 151.55, 128.59, 124.56, 124.42, 124.37, 120.79, 113.08, 111.33, 111.17, 102.27, 68.31, 56.08, 54.88, 53.79, 28.58, 26.48, 23.42, 23.20. U-HR-MS (ESI) *m/z*: Calcd. for C<sub>23</sub>H<sub>28</sub>NO<sub>4</sub> [M+H]<sup>+</sup>: 382.2013. Found: 382.2008.

**8-methoxy-3-((5-(piperidin-1-yl)pentyl)oxy)-6H-benzo[c]chromen-6-one(UD-5b).** Yellow-white solid, yield 96.95%. <sup>1</sup>H NMR (400 MHz, Chloroform-*d*) δ 7.92 (d, *J*=8.9 Hz, 1H), 7.85 (d, *J*=8.8 Hz, 1H), 7.75 (d, *J*=2.8 Hz, 1H), 7.37 (dd, *J*=8.8, 2.8 Hz, 1H), 6.89 (dd, *J*=8.8, 2.5 Hz, 1H), 6.83 (d, *J*=2.5 Hz, 1H), 4.02 (t, *J*=6.3 Hz, 2H), 3.92 (s, 3H), 2.65 (s, 4H), 2.60–2.51 (m, 2H), 1.86 (dt, *J*=14.5, 6.5 Hz, 2H), 1.77 (dq, *J*=13.1, 7.7, 6.8 Hz, 6H), 1.58–1.46 (m, 4H). <sup>13</sup>C NMR (101 MHz, Chloroform-*d*) δ 161.64, 160.09, 159.08, 151.56, 128.68, 124.44, 123.12, 122.80, 120.88, 112.67, 111.15, 110.92, 102.08, 68.14, 58.90, 55.75, 54.32, 28.89, 25.88, 25.09, 24.03, 23.85. U-HR-MS (ESI) *m/z*: Calcd. for C<sub>24</sub>H<sub>30</sub>NO<sub>4</sub> [M+H]<sup>+</sup>: 396.2169. Found: 396.2164.

**3-((5-(Azepan-1-yl)pentyl)oxy)-8-methoxy-6H-benzo[c]chromen-6-one(UD-5c).** Yellow solid, yield 92.05%. <sup>1</sup>H NMR (400 MHz, Chloroform-*d*) δ 7.92 (d, *J*=8.9 Hz, 1H), 7.85 (d, *J*=8.9 Hz, 1H), 7.75 (d, *J*=2.8 Hz, 1H), 7.37 (dd, *J*=8.8, 2.8 Hz, 1H), 6.89 (dd, *J*=8.8, 2.5 Hz, 1H), 6.82 (d, *J*=2.5 Hz, 1H), 4.02 (t, *J*=6.2 Hz, 2H), 3.92 (s, 3H), 3.03–2.96 (m, 4H), 2.85–2.77 (m, 2H), 1.86 (q, *J*=7.1 Hz, 8H), 1.69 (p, *J*=2.7 Hz, 4H), 1.54 (ddd, *J*=15.2, 9.2, 6.3 Hz, 2H). <sup>13</sup>C NMR (101 MHz, Chloroform-*d*) δ 161.63, 160.01, 159.10, 151.53, 128.64, 124.43, 123.16, 122.83, 120.87, 112.61, 111.20, 110.94, 102.12, 68.02, 57.78, 55.76, 55.03, 28.72, 26.96, 25.46, 23.80. U-HR-MS (ESI) *m/z*: Calcd. for C<sub>25</sub>H<sub>32</sub>NO<sub>4</sub> [M+H]<sup>+</sup>: 410.2326. Found: 410.2320.

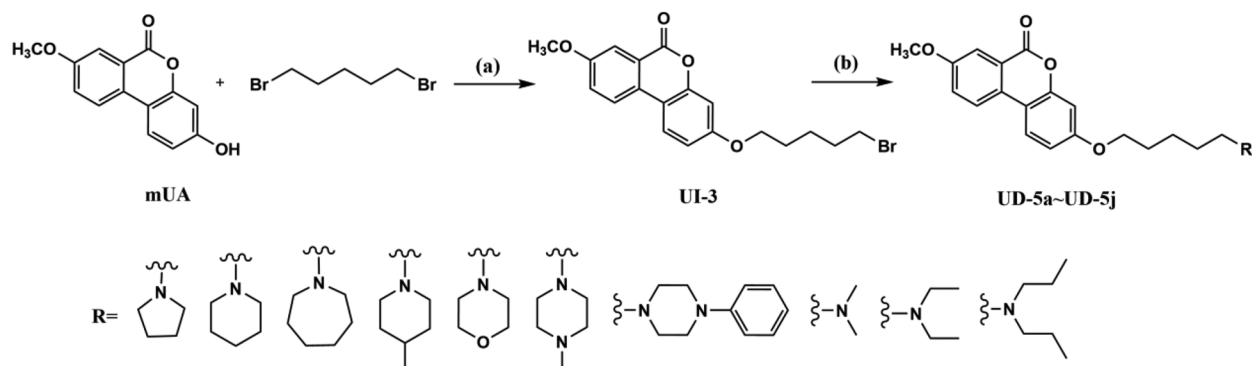
**8-methoxy-3-((5-(4-methylpiperidin-1-yl)pentyl)oxy)-6H-benzo[c]chromen-6-one(UD-5d).** Light yellow solid, yield 86.80%. <sup>1</sup>H NMR (400 MHz, Chloroform-*d*) δ 7.94 (d, *J*=8.9 Hz, 1H), 7.87 (d, *J*=8.8 Hz,

58.67, 55.77, 53.87, 33.56, 30.50, 28.93, 26.25, 24.08, 21.72. U-HR-MS (ESI)  $m/z$ : Calcd. for  $C_{25}H_{33}NO_4$   $[M+H]^+$ : 410.2326. Found: 410.2320.

Chemical reaction scheme showing the synthesis of UD-2a from mUA (3-methoxy-6-hydroxyfluoren-9-one) and 1-(2-chloroethyl)pyrrolidine hydrochloride. The reaction is labeled (a) and involves NaH and DMF at 100 °C for 24 h.

[illegible]

**Scheme 4.** Reagents and conditions: (a)  $K_2CO_3$ , acetone, 62 °C. (b)  $K_2CO_3$ , KI, acetonitrile, 82 °C



2.5Hz, 1H), 6.84 (d,  $J=2.5$ Hz, 1H), 4.02 (t,  $J=6.4$ Hz, 2H), 3.93 (s, 3H), 3.73 (t,  $J=4.7$ Hz, 4H), 2.46 (d,  $J=5.2$ Hz, 4H), 2.43–2.34 (*m*, 2H), 1.85 (*p*,  $J=6.7$ Hz, 2H), 1.64–1.46 (*m*, 4H).  $^{13}\text{C}$  NMR (151 MHz, Chloroform-*d*)  $\delta$  161.85, 160.37, 159.37, 151.87, 128.94, 124.69, 123.31, 123.00, 121.19, 112.99, 111.40, 111.21, 102.29, 68.46, 67.16, 59.14, 55.96, 53.98, 29.19, 26.46, 24.17. U-HR-MS (ESI)  $m/z$ : Calcd for  $\text{C}_{23}\text{H}_{28}\text{NO}_5$  [ $\text{M}+\text{H}$ ] $^+$ : 398.1962. Found: 398.1958.

**8-methoxy-3-((5-(4-methylpiperazin-1-yl)pentyl)oxy)-6H-benzo[*c*]chromen-6-one(UD-5f).** Yellow solid, yield 62.52%. <sup>1</sup>H NMR (400 MHz, Chloroform-*d*) δ 7.92 (d, *J*=8.9 Hz, 1H), 7.86 (d, *J*=8.9 Hz, 1H), 7.76 (d, *J*=2.8 Hz, 1H), 7.37 (dd, *J*=8.8, 2.8 Hz, 1H), 6.89 (dd, *J*=8.8, 2.5 Hz, 1H), 6.83 (d, *J*=2.5 Hz, 1H), 4.02 (t, *J*=6.2 Hz, 2H), 3.93 (s, 3H), 2.99 (s, 8H), 2.71–2.63 (m, 2H), 2.57 (s, 3H), 1.91–1.80 (m, 2H), 1.80–1.70 (m, 2H), 1.54 (tt, *J*=10.0, 6.2 Hz, 2H). <sup>13</sup>C NMR (101 MHz, Chloroform-*d*) δ 161.64, 160.00, 159.12, 151.54, 128.64, 124.46, 123.19, 122.84, 120.88, 112.69, 111.23, 110.96, 102.08, 68.03, 57.47, 55.77, 53.23, 50.97, 44.68, 28.73, 25.44, 23.70. U-HR-MS (ESI) *m/z*: Calcd. for C<sub>24</sub>H<sub>31</sub>N<sub>3</sub>O<sub>4</sub> [*M*+H]<sup>+</sup>: 411.2278. Found: 411.2278.

**8-methoxy-3-((5-(4-phenylpiperazin-1-yl)pentyl)oxy)-6H-benzo[*c*]chromen-6-one(UD-5g).** White solid, yield 85.69%. <sup>1</sup>H NMR (400 MHz, Chloroform-*d*) δ 7.92 (d, *J*=8.9 Hz, 1H), 7.85 (d, *J*=8.8 Hz, 1H), 7.76 (d, *J*=2.8 Hz, 1H), 7.37 (dd, *J*=8.8, 2.8 Hz, 1H), 7.26 (d, *J*=15.8 Hz, 1H), 6.97–6.81 (*m*, 6H), 4.03 (t, *J*=6.4 Hz, 2H), 3.92 (*s*, 3H), 3.22 (t, *J*=5.0 Hz, 4H), 2.63 (t, *J*=5.0 Hz, 4H), 2.49–2.41 (*m*, 2H), 1.87 (*p*, *J*=6.7 Hz, 2H), 1.70–1.52 (*m*, 4H). <sup>13</sup>C NMR (101 MHz, Chloroform-*d*) δ 161.66, 160.15, 159.11, 151.62, 151.32, 129.12, 128.72, 124.49, 123.12, 122.80, 120.93, 119.70, 116.05, 112.78, 111.16, 110.93, 102.04, 68.25, 58.58, 55.77, 53.34, 49.13, 29.03, 26.66, 24.08. U-HR-MS (ESI) *m/z*: Calcd. for C<sub>20</sub>H<sub>33</sub>N<sub>2</sub>O<sub>4</sub> [M+H]<sup>+</sup>: 473.2435. Found: 473.2429.

### Cell viability assay

The CCK-8 assay was used to determine cell viability. The density of DU145 and T24 cells was adjusted to  $1 \times 10^4$  cells/mL, and the density of HepG2 cells was adjusted to 8,000 cells/mL using the fresh complete medium. Subsequently, 100  $\mu$ L of cell suspension were added into 96-well plates and incubated at 37°C with 5% CO<sub>2</sub> for 24 h. Furthermore, 100  $\mu$ L of compound solution with different concentrations was re-added to each well and incubated for an additional 48 h. The drug solution was aspirated, and the wells were rinsed with 100  $\mu$ L of basal medium containing 10% CCK-8 reagent. The plate was placed in an electrically heated incubator at 37°C for incubation. After 30 min, the absorbance at 450 nm was measured using a multi-functional imaging microplate reader.

The IC<sub>50</sub> was calculated using GraphPad Prism software (version 8.0), and each concentration was repeated at least thrice.

### Colony assay

HepG2 cells were placed into 6-well plates at  $5 \times 10^3$  cells per well and incubated for 24 h. Subsequently, the cells were treated with compound UD-4c at concentrations of 0, 2, 4, and  $10 \mu\text{M}$  for 48 h. The 6-well plates were replaced every two days for six days, after which the cells were fixed with 4% paraformaldehyde for 40 min. Subsequently, 1 ml of 1% crystalline violet staining solution was added for 30 min at room temperature and photographed and recorded.

### Hoechst 33,258 staining

HepG2 cells were placed into 6-well plates at  $1.8 \times 10^5$  cells per well and incubated for 24 h. Subsequently, the cells were treated with compound UD-4c at concentrations of 0, 2, 4, and  $10 \mu\text{M}$  for 48 h. After removal and rinsing, 1 ml of Hoechst 33258 staining solution was added to each well. The samples were incubated at  $37^\circ\text{C}$  for 30 min to avoid light staining. Subsequently, the staining solution was aspirated and rinsed twice. The samples were photographed using an inverted fluorescence microscope.

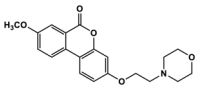
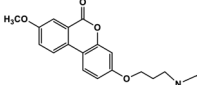
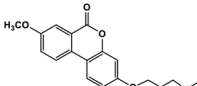
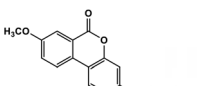
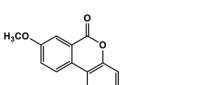
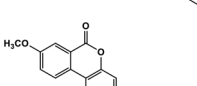
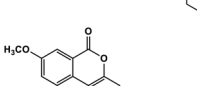
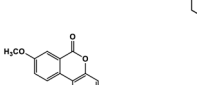
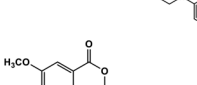
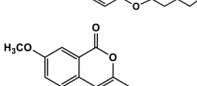
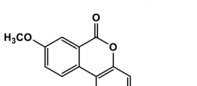
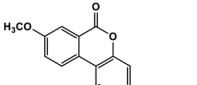
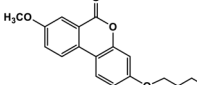
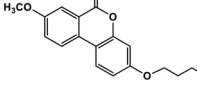
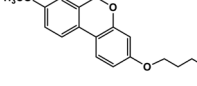
### Cell apoptosis assay

HepG2 cells were placed into 6-well plates at  $2.5 \times 10^5$  cells per well and incubated for 24h. Subsequently, the cells were treated with compound UD-4c at concentrations of 0, 4, 10, and 20  $\mu\text{M}$  for 48h, followed by wetting and digestion, and all cells were collected. We added 100  $\mu\text{L}$  of pre-chilled  $1 \times$  Annexin V Binding Buffer to each group, and the cells were resuspended. Each group was added with 5  $\mu\text{L}$  each of Annexin V-FITC and PI staining solution, vortexed and mixed, and stained at room temperature for 15min. Subsequently, 400  $\mu\text{L}$  of pre-chilled  $1 \times$  Annexin V Binding Buffer working solution was added and detected using a flow cytometer.

### Cell cycle assay

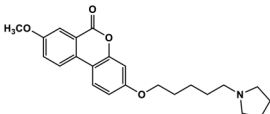
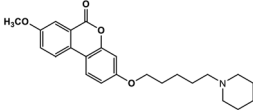
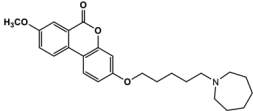
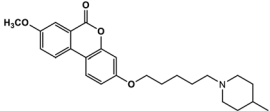
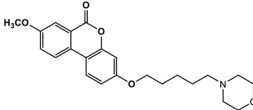
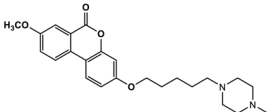
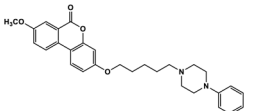
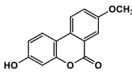
HepG2 cells were placed into 6-well plates at  $2.0 \times 10^5$  cells per well and incubated for 24 h. Subsequently, the cells were treated with compound UD-4c at concentrations of 0, 4, 10, and  $20 \mu\text{M}$  for 48 h, washed, digested, and centrifuged. Subsequently, 1 ml of PBS

**Table 1.** Anti-proliferative activity of newly synthesised urolithin derivatives, mUA and positive drugs against the tested cancer cell lines.

Compound	Structure	IC <sub>50</sub> (μM) <sup>a</sup>		
		HepG2	T24	DU145
UD-2a		ND	ND	ND
UD-3a		7.17 ± 0.26	17.03 ± 0.26	16.99 ± 0.94
UD-3b		5.57 ± 0.16	24.76 ± 0.72	18.29 ± 0.49
UD-3c		7.92 ± 0.16	21.52 ± 0.38	36.45 ± 1.27
UD-3d		7.06 ± 0.34	53.92 ± 1.13	92.96 ± 3.33
UD-3e		20.99 ± 0.33	170 ± 5.00	39.92 ± 2.42
UD-3f		11.61 ± 0.57	23.02 ± 0.23	15.48 ± 0.30
UD-3g		ND	ND	ND
UD-4a		9.30 ± 0.11	31.95 ± 0.19	20.54 ± 1.65
UD-4b		6.60 ± 0.11	20.73 ± 0.44	15.78 ± 0.61
UD-4c		4.66 ± 0.12	19.77 ± 0.49	17.38 ± 0.15
UD-4d		8.31 ± 0.29	34.43 ± 0.96	18.08 ± 0.21
UD-4e		61.01 ± 5.41	ND	66.06 ± 4.20
UD-4f		10.33 ± 0.43	34.43 ± 0.21	34.38 ± 0.80
UD-4g		89.56 ± 3.74	ND	390.90 ± 18.67

(Continued)

Table 1. Continued.

Compound	Structure	IC <sub>50</sub> (μM) <sup>a</sup>		
		HepG2	T24	DU145
UD-5a		6.38 ± 0.24	21.78 ± 0.10	17.75 ± 0.91
UD-5b		5.10 ± 0.02	26.66 ± 0.51	10.13 ± 0.36
UD-5c		4.95 ± 0.03	17.36 ± 0.41	14.14 ± 0.32
UD-5d		8.54 ± 0.28	23.57 ± 0.18	29.63 ± 0.44
UD-5e		56.79 ± 4.01	ND	60.07 ± 0.31
UD-5f		8.58 ± 0.13	24.46 ± 0.08	17.96 ± 0.57
UD-5g		ND	ND	ND
mUA		11.36 ± 0.92	49.76 ± 0.44	55.84 ± 0.51
Cisplatin	—	—	14.49 ± 0.13	2.95 ± 0.22
Sorafenib	—	7.76 ± 0.12	—	—

a: after treating the cells with different concentrations of the test compounds for 48 h, the inhibitory cell proliferation activity was measured and expressed as the half-inhibitory concentration (IC<sub>50</sub>). Data are presented as the Mean ± SD. All experiments were carried out at least three independent times.

Table 2. IC<sub>50</sub> of UD-4c treated HepG2 cells and HK-2 cells after 48 h.

Cell line	IC <sub>50</sub> (μM)
HK-2	22.59 ± 0.58
HepG2	4.66 ± 0.12

was added, and the cells were resuspended. The suspended cell was added to 3 ml of pre-chilled anhydrous ethanol at −20 °C several times. The cells were centrifuged, and 500 μL of PI/Rnase A staining solution was added, vortexed, mixed, and stained for 40 min at room temperature, protected from light, and detected using a flow cytometer.

## Result and discussion

### Chemistry

Schemes 1–5 depict the overall synthetic routes of urolithin derivatives. We synthesised mUA from resorcinol and 2-bromo-5-methoxybenzoic acid, which were first reacted to form an ester under the action of NaOH. Subsequently, mUA was synthesised in a reaction catalysed by Cu<sup>2+</sup>, resulting in a 38.79% yield (Scheme 1).

In Scheme 2, mUA was synthesised by an alkylation reaction with 4-(2-chloroethyl)morpholine hydrochloride in the presence of K<sub>2</sub>CO<sub>3</sub> to synthesise the derivative UD-2a in an 87.90% yield. In Schemes 3, 4, and 5, mUA was alkylated with 1,3-dibromopropane, 1,4-dibromobutane, and 1,5-dibromopentane, respectively, catalysed by K<sub>2</sub>CO<sub>3</sub> to generate urolithin derivative intermediates UI-1, UI-2, and UI-3, and intermediates UI-1, UI-2, and UI-3 were alkylated with a series of cyclic amine group terminals, respectively, catalysed by K<sub>2</sub>CO<sub>3</sub> and KI to generate a series of derivatives, UD-1, UI-2, and UI-3. The amination reaction produced a series of derivatives, UD-3a~UD-3g, UD-4a~UD-4g, and UD-5a~UD-5g, with yields ranging from 44.81%–81.52%, 35.25%–91.37%, and 49.99%–97.42%, respectively.

### In vitro cytotoxicity

The Cell Counting Kit-8 (CCK-8 assay) assay was used to assess the effects of all urolithin derivatives on HepG2 (human hepatocellular carcinoma cells), T24 (human bladder metastatic cell carcinoma cells), and DU145 (human bladder carcinoma cells) proliferation. The clinical drug sorafenib was used as a positive control for HepG2 cells, while cisplatin was used as a positive control for T24



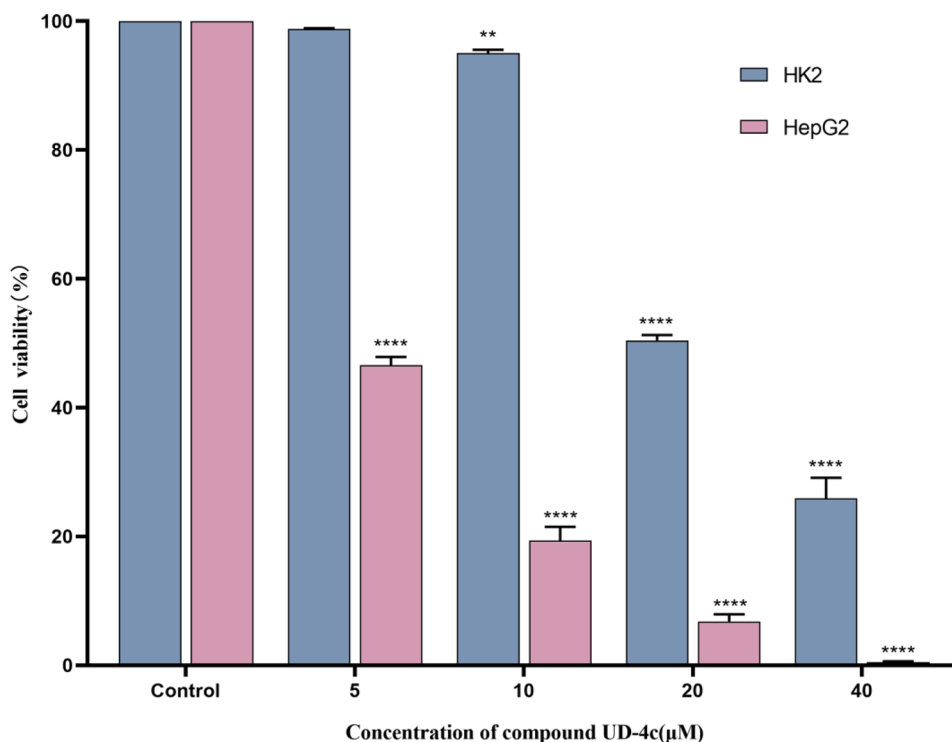


**Figure 1.** Inhibition rate of HepG2 and HK-2 cells treated with different concentrations of UD-4c solution after 48h. Note: Compared with control group, \* $P < 0.05$ , \*\* $P < 0.01$ , \*\*\* $P < 0.001$ , \*\*\*\* $P < 0.0001$ .

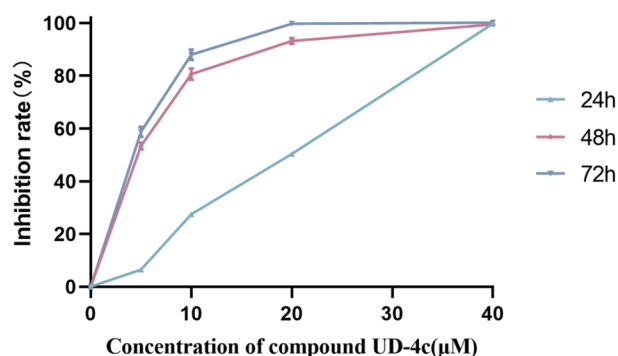


**Figure 2.** The inhibition rates of HepG2 cells treated with different concentrations of derivative UD-4c solution for 24, 48 and 72h, respectively.

and DU145 cells. The cytotoxicity of the derivatives is expressed as half-inhibitory concentration  $IC_{50}$  in Table 1, and  $IC_{50}$  was calculated using linear regression analysis of the concentration-inhibition curves for each derivative. The results revealed that most derivatives inhibited DU145, T24, and HepG2 cell proliferation to varying degrees, and the activity was superior to that of the parent compound mUA.

For DU145 cells, the  $IC_{50}$  after 48h of mUA treatment was  $55.84 \pm 0.51 \mu M$ . Table 1 reveals that the  $IC_{50}$  of all derivatives except derivatives UD-2a, UD-3d, UD-3g, UD-4e, UD-4g, UD-5e, and UD-5g was  $< 55.84 \pm 0.51 \mu M$ , and the anti-proliferative activity was better than that of mUA, among which UD-5b exhibited the best anti-proliferative activity with an  $IC_{50}$  of  $10.13 \pm 0.36 \mu M$ . However, the  $IC_{50}$  of all derivatives was greater than that of the positive drug cisplatin ( $IC_{50} = 2.95 \pm 0.22 \mu M$ ), and the anti-proliferative activity was weaker than that of cisplatin.

For T24 cells, the  $IC_{50}$  after 48h of mUA treatment was  $49.76 \pm 0.44 \mu M$ . Table 1 reveals that the  $IC_{50}$  of all derivatives except derivatives UD-2a, UD-3d, UD-3e, UD-3g, UD-4e, UD-4g, and UD-5e, UD-5g were  $< 49.76 \pm 0.44 \mu M$ , and the anti-proliferative activity was better than that of mUA. However, the  $IC_{50}$  of all derivatives was higher than that of the cisplatin ( $IC_{50} = 14.49 \pm 0.13 \mu M$ ). The proliferative activity of UD-3a was the best, with  $IC_{50}$  of  $17.03 \pm 0.26 \mu M$ .

For HepG2 cells, the  $IC_{50}$  of mUA treatment for 48h was  $11.36 \pm 0.92 \mu M$ . Table 1 reveals the  $IC_{50}$  of all derivatives was  $< 11.36 \pm 0.92 \mu M$ , except for derivatives UD-2a, UD-3e, UD-3f, UD-3g, UD-3h, UD-4e, UD-4g, UD-5e, UD-5g, and the anti-proliferative activity was better than that of mUA. The  $IC_{50}$  of most derivatives was  $< 10 \mu M$  after 48h treatment of HepG2 cells. Compared with the positive drug sorafenib ( $IC_{50} = 7.76 \pm 0.12 \mu M$ ), the derivatives UD-3a ( $IC_{50} = 7.17 \pm 0.26 \mu M$ ), UD-3d ( $IC_{50} = 7.06 \pm 0.34 \mu M$ ), UD-4b ( $IC_{50} = 6.60 \pm 0.11 \mu M$ ), and UD-5a ( $IC_{50} = 6.38 \pm 0.24 \mu M$ ) inhibited HepG2 cell proliferation slightly better than Sorafenib. The derivatives UD-3b ( $IC_{50} = 5.57 \pm 0.16 \mu M$ ), UD-4c ( $IC_{50} = 4.66 \pm 0.12 \mu M$ ), UD-5b ( $IC_{50} = 5.10 \pm 0.02 \mu M$ ), and UD-5c ( $IC_{50} = 4.95 \pm 0.03 \mu M$ ) inhibited the HepG2 cell proliferation significantly better than Sorafenib, while derivative UD-4c exhibited the best anti-proliferative activity.

Derivatives UD-3g, UD-4g, and UD-5g with N-phenylpiperazine at the amino-terminal demonstrated no anti-proliferative activity against DU145, T24, and HepG2, while derivatives UD-3f, UD-4f, and UD-5f with N-methyl piperazine at the amino-terminal demonstrated better anti-proliferative activity against the above three cancer cells because the spatial site resistance of phenyl in N-phenylpiperazine is higher than that of methyl in N-methyl piperazine. Therefore, the steric hindrance of the amino-terminal should be moderate. UD-2a demonstrated no anti-proliferative

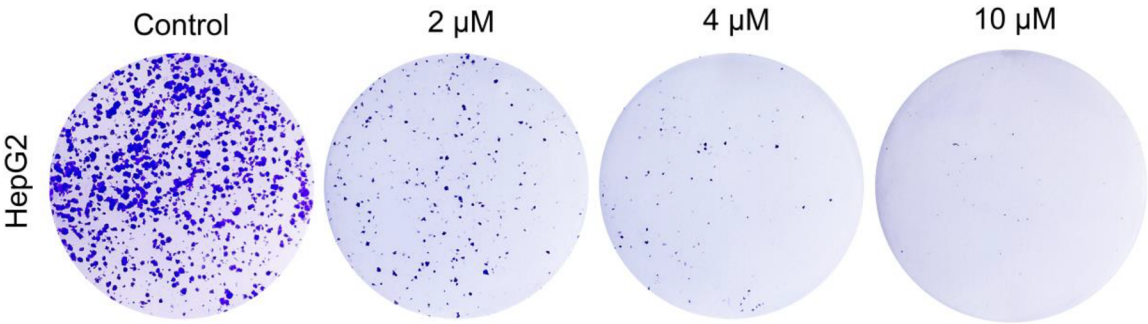


**Figure 3.** Representative pictures of cell colony formation by crystalline violet staining of HepG2 cells treated with different concentrations of derivative UD-4c for 48h and continued to be cultured for 6 d.

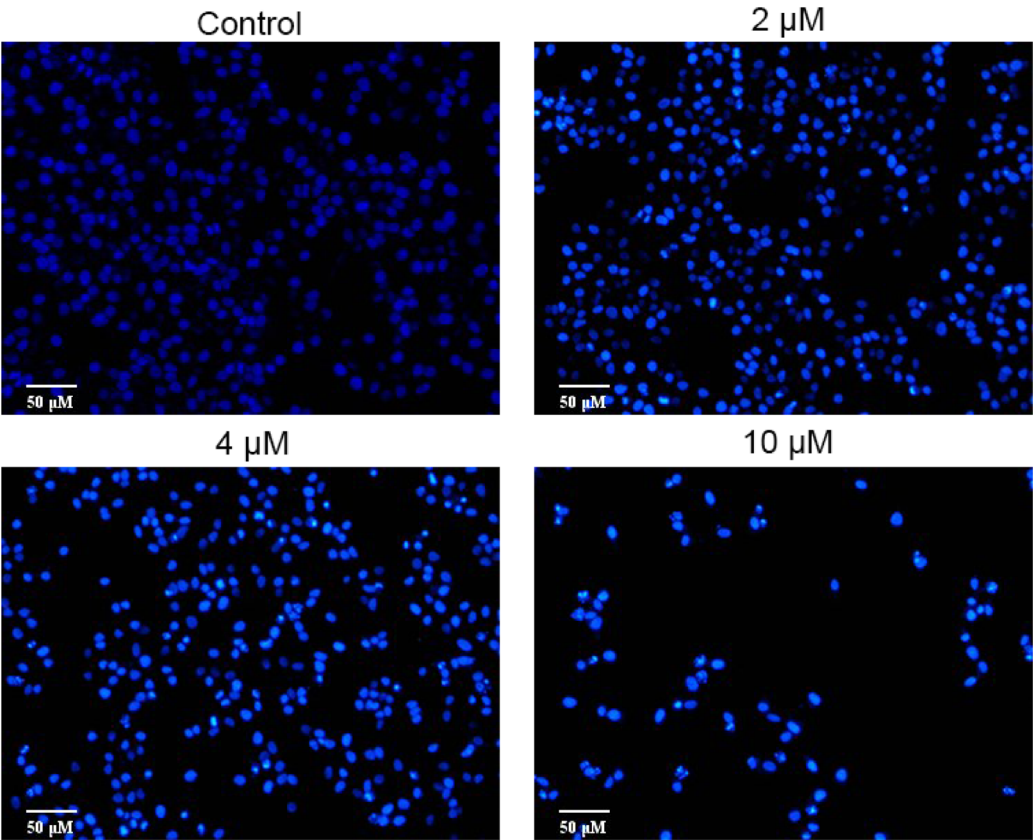


**Figure 4.** Hoechst33258 staining of HepG2 cells treated with different concentrations of derivative UD-4c for 48h.

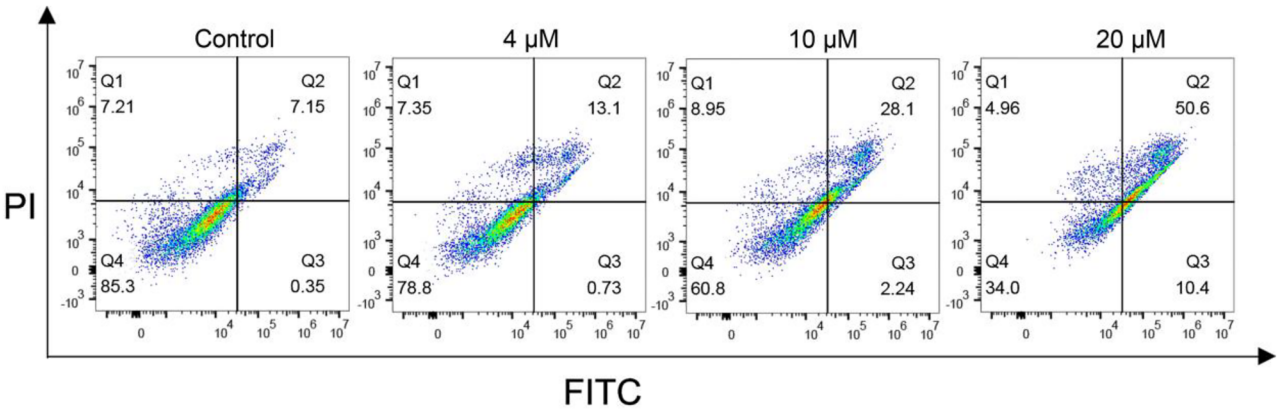


**Figure 5.** Representative pictures of Annexin V-FITC/PI fluorescence double staining method to detect apoptosis of HepG2 cells after 48h by different concentrations of derivative UD-4c.

activity against DU145, T24, and HepG2. However, UD-3e, UD-4e, and UD-5e demonstrated better anti-proliferative activity than UD-2a, while the amino-terminals of UD-2a, UD-3e, UD-4e, and UD-5e are all morpholine. The only difference lies in the number of carbon atoms in the flexible carbon chain, which are two, three, four, and five, respectively. This indicates that the flexible carbon chain should be moderate, with the carbon atoms more than two.

Table 2 and Figure 1. Illustrate the toxicity of the derivative UD-4c on human renal cortical proximal tubule epithelial cells (HK-2). Compared with HepG2 cells, UD-4c inhibited HepG2 growth much more than HK-2 and was less toxic to normal human cells.

The anti-proliferative activity of urolithin derivatives against HepG2 cells was significantly better than that of DU145 and T24 cells, and the derivative UD-4c exhibited the best activity. We subsequently used HepG2 cells to investigate the potential antitumor mechanism of derivative UD-4c based on the significant anti-proliferative activity and high selectivity of UD-4c against human hepatocellular carcinoma HepG2 cells.

#### Effect of compound UD-4c on growth inhibition in human hepatoma cancer cell lines HepG2

We used CCK-8 assay to measure the inhibition rate of derivative UD-4c acting on HepG2 cells for 24, 48, and 72 h. Figure 2 depicts the results. Derivative UD-4c significantly inhibited HepG2 cell proliferation dose- and time-dependently, and to further evaluate the anti-proliferative activity of derivative UD-4c

on HepG2 cells, a plate clone formation assay was performed. Figure 3 depicts the results. Compared with the control group, the number of clone-forming cell colonies and cells per colony decreased as the derivative UD-4c concentration increased, and UD-4c significantly reduced HepG2 cell colony formation, especially in the high-dose group.

#### Effect of compound UD-4c on apoptosis in HepG2 cells

We performed apoptosis-related experiments to investigate whether the derivative UD-4c could induce apoptosis in HepG2 cells. Initially, we used Hoechst 33258 staining to qualitatively detect the ability of derivative UD-4c to promote apoptosis of HepG2 cells. The results are illustrated in Figure 4. Normal cells in the control group were stained blue, exhibited normal morphological structure, and were round or oval. More cells were apoptotic after UD-4c treatment for 48 h. The nuclei of apoptotic cells were stained bright blue and concentrated in the middle or side of the cells. Some were distributed in fragments inside the cells. The percentage of bright blue cells increased with concentration. Subsequently, we used the Annexin V-FITC&PI double staining method to quantify the apoptosis rate of derivative UD-4c treated HepG2 cells after 48 h. The results are depicted in Figures 5 and 6, where the upper right part is the late apoptotic or necrotic cells, and the lower right part is the early or middle apoptotic cells. Compared with the control group, the apoptosis rate of late apoptotic or necrotic cells and early or mid-stage apoptotic cells was higher than that of the

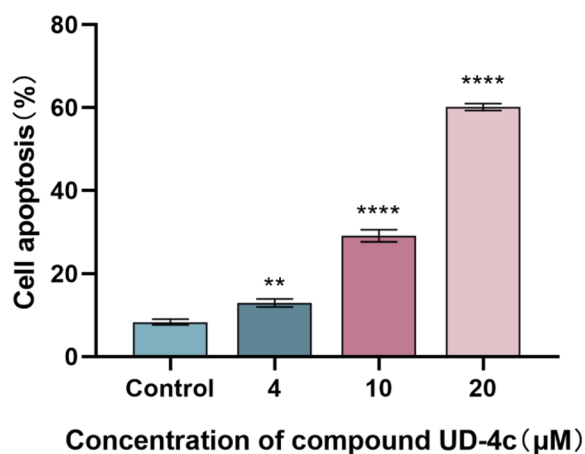


**Figure 6.** Quantitative analysis of early and late apoptosis rates of derivative UD-4c treated HepG2 cells after 48 h by flow cytometry. Note: Compared with the control group, \* $P < 0.05$ , \*\* $P < 0.01$ , \*\*\* $P < 0.001$ , \*\*\*\* $P < 0.0001$ .

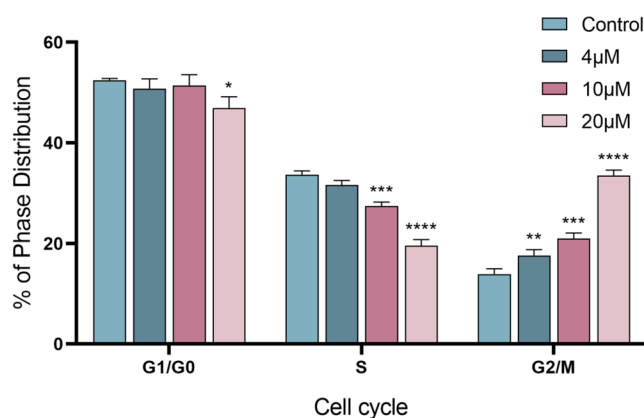


**Figure 8.** Quantification of the percentage of cell cycle distribution of HepG2 cells treated with different concentrations of derivative UD-4c solution for 48 h. Note: Compared with the control group, \* $P < 0.05$ , \*\* $P < 0.01$ , \*\*\* $P < 0.001$ , \*\*\*\* $P < 0.0001$ .

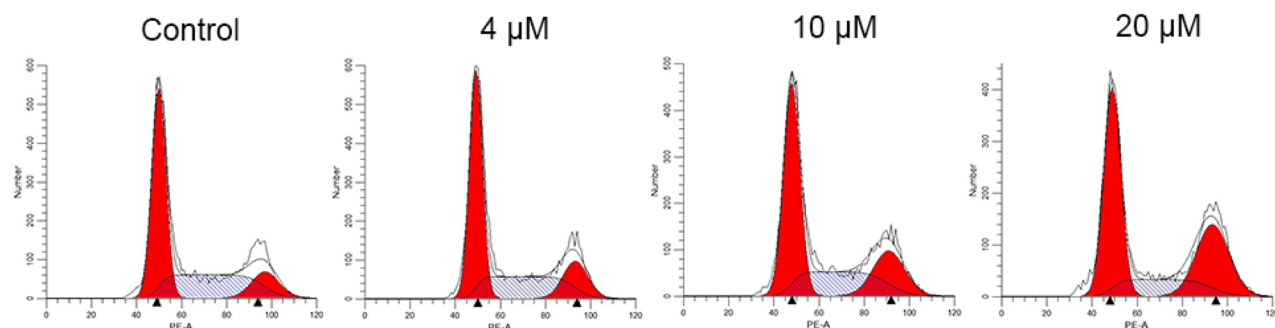


**Figure 7.** PI staining method to detect the cell cycle distribution of HepG2 cells treated with different concentrations of derivative UD-4c solution for 48 h.

control group, and the apoptosis rate increased with concentration. The qualitative and quantitative analyses revealed that the derivative UD-4c induced apoptosis in HepG2 cells dose-dependently.

### Effect of compound UD-4c on cell cycle in HepG2 cells

Cell cycle analysis was used to investigate the anti-proliferative activity of the derivative UD-4c to confirm if it correlated with HepG2 cell cycle arrest. HepG2 cells were treated with the indicated concentrations of UD-4c for 48h, stained with PI(Propidium Iodide) staining solution, and assayed using a flow cytometer. Figures 7 and 8 depict the result. Compared with the control group, the percentage of HepG2 cells in the G2/M phase gradually increased, from 12.73% to 16.36%, 20.77%, and 32.4%, respectively, while the cells in the S phase gradually decreased from 34.45% to 30.61%, 27.26%, and 18.16%, respectively. The change of cells in the G1/G0 phase was nonobvious; therefore, the derivative UD-4c induced HepG2 cells in the G2/M phase arrest dose-dependently, thus inhibiting HepG2 cell proliferation.

### Conclusions

We synthesised 22 structurally new urolithin derivatives, evaluated their *in vitro* antitumor activity, and preliminary investigated the potential mechanism by which the derivative UD-4c inhibits hepatocellular carcinoma cell proliferation. In vitro, anti-proliferative experiments revealed that most derivatives exhibited good anti-proliferative activity against DU145, T24, and HepG2 cells. Additionally, they were more effective than the parent compound mUA and exhibited highly selective cytotoxicity against HepG2 cells. The derivative UD-4c exhibited the most potent proliferation inhibitory effect on HepG2 cells, significantly better than the first-line drug sorafenib for hepatocellular carcinoma treatment. The introduction of the amine structure significantly improved the anti-cancer activity. The preliminary investigation of the mechanism revealed that the derivative UD-4c could induce cell cycle delay, block HepG2 cells in the G2/M phase, and dose-dependently induce apoptosis of HepG2 cells, thus inhibiting HepG2 cell proliferation and exerting therapeutic effects on cancer while the toxicity of UD-4c to human normal cells HK-2 was much less than that of human hepatocellular carcinoma HepG2 cells.

This research broadens the prospects of study on drugs for the treatment of liver cancer. In the future, we will further study the cytotoxicity of the derivative UD-4c on other hepatocellular carcinoma cells. Meanwhile, we hypothesise that the anti-liver cancer effect of UD-4c may be related to its induction of oxidative stress, leading to mitochondrial apoptosis, and the regulation of apoptosis by affecting the ROS/AKT/FoxO3a axis, thus promoting the apoptosis of liver cancer cells. Meanwhile, we will explore the anti-liver cancer action targets and signalling pathways of UD-4c by combining experimental techniques such as molecular docking and western-blot, and conduct *in vivo* verification using mice. We aim to deeply elucidate the anti-liver cancer mechanism of UD-4c and strive to provide potential therapeutic drugs for clinical practice.

### Authors contributions

The conception and design, or analysis and interpretation of the data: Mi Tian, Lirong Zhao, Yu Lan, Chen Li, Yipeng Ling, Benhong Zhou

The drafting of the paper, revising it critically for intellectual content: Mi Tian, Lirong Zhao, Yu Lan, Chen Li, Yipeng Ling, Benhong Zhou

The final approval of the version to be published: Mi Tian, Lirong Zhao, Yu Lan, Chen Li, Yipeng Ling, Benhong Zhou

All authors agree to be responsible for all aspects of the work

### Disclosure statement

No potential conflict of interest was reported by the author(s).

### Funding

The financial support of this study was obtained from the National Natural Science Foundation of China.(NO.31770381)

### Data availability statement

The datasets presented in the current study are available from the corresponding author upon reasonable request.

### References

1. Adewole KE. Nigerian antimalarial plants and their anticancer potential: a review. *J Integr Med.* 2020;18(2):92–113.
2. Plaza M, Batista ÂG, Cazarin CBB, Sandahl M, Turner C, Östman E, Maróstica Júnior MR. Characterization of antioxidant polyphenols from *Myrciaria jaboticaba* peel and their effects on glucose metabolism and antioxidant status: a pilot clinical study. *Food Chem.* 2016;211:185–197.
3. Pajari A-M, Päiväranta E, Paavola L, Vaara E, Koivumäki T, Garg R, Heiman-Lindh A, Mutanen M, Marjomäki V, Ridley AJ, et al. Ellagitannin-rich cloudberry inhibits hepatocyte growth factor-induced cell migration and phosphatidylinositol 3-kinase/AKT activation in colon carcinoma cells and tumors in Min mice. *Oncotarget.* 2016;7(28):43907–43923.
4. Park KH, Yin J, Yoon KH, Hwang YJ, Lee MW. Antiproliferative effects of new dimeric ellagitannin from *Cornus alba* in prostate cancer cells including apoptosis-related s-phase arrest. *Molecules.* 2016;21(2):137.
5. Gontijo DC, Gontijo PC, Brandão GC, Diaz MAN, de Oliveira AB, Fietto LG, Leite JPV. Antioxidant study indicative of antibacterial and antimutagenic activities of an ellagitannin-rich aqueous extract from the leaves of *Miconia latecrenata*. *J Ethnopharmacol.* 2019;236:114–123.
6. Bedoya LM, Abad MJ, Sánchez-Palomino S, Alami J, Bermejo P. Ellagitannins from *Tuberaria lignosa* as entry inhibitors of HIV. *Phytomedicine.* 2010;17(1):69–74.
7. Espín JC, Larrosa M, García-Conesa MT, Tomás-Barberán F. Biological significance of urolithins, the gut microbial ellagic acid-derived metabolites: the evidence so far. *Evidence-Based Complementary and Alternative Medicine.* 2013;2013:1–15.
8. Cerdá B, Tomás-Barberán FA, Espín JC. Metabolism of antioxidant and chemopreventive ellagitannins from strawberries, raspberries, walnuts, and oak-aged wine in humans: Identification of biomarkers and individual variability. *J Agric Food Chem.* 2005;53(2):227–235.
9. Seeram NP, Henning SM, Zhang Y, Suchard M, Li Z, Heber D. Pomegranate juice ellagitannin metabolites are present in



- human plasma and some persist in urine for up to 48 hours. *J Nutr.* 2006;136(10):2481–2485.
10. García-Villalba R, Beltrán D, Espín JC, Selma MV, Tomás-Barberán FA. Time course production of urolithins from ellagic acid by human gut microbiota. *J Agric Food Chem.* 2013;61(37):8797–8806.
  11. Nuñez-Sánchez MA, García-Villalba R, Monedero-Saiz T, García-Talavera NV, Gómez-Sánchez MB, Sánchez-Álvarez C, García-Albert AM, Rodríguez-Gil FJ, Ruiz-Marín M, Pastor-Quirante FA, et al. Targeted metabolic profiling of pomegranate polyphenols and urolithins in plasma, urine and colon tissues from colorectal cancer patients. *Mol Nutr Food Res.* 2014;58(6):1199–1211.
  12. García-Villalba R, Espín JC, Tomás-Barberán FA. Chromatographic and spectroscopic characterization of urolithins for their determination in biological samples after the intake of foods containing ellagitannins and ellagic acid. *J Chromatogr A.* 2016;1428:162–175.
  13. Bialonska D, Kasimsetty SG, Khan SI, Ferreira D. Urolithins, intestinal microbial metabolites of pomegranate ellagitannins, exhibit potent antioxidant activity in a cell-based assay. *J Agric Food Chem.* 2009;57(21):10181–10186.
  14. Giménez-Bastida JA, González-Sarriás A, Larrosa M, Tomás-Barberán F, Espín JC, García-Conesa M-T. Ellagitannin metabolites, urolithin A glucuronide and its aglycone urolithin A, ameliorate TNF- $\alpha$ -induced inflammation and associated molecular markers in human aortic endothelial cells. *Mol Nutr Food Res.* 2012;56(5):784–796.
  15. Kiss AK, Granica S, Stolarczyk M, Melzig MF. Epigenetic modulation of mechanisms involved in inflammation: influence of selected polyphenolic substances on histone acetylation state. *Food Chem.* 2012;131(3):1015–1020.
  16. Xu J, Yuan C, Wang G, Luo J, Ma H, Xu L, Mu Y, Li Y, Seeram NP, Huang X, et al. Urolithins Attenuate LPS-induced neuroinflammation in BV2 Microglia via MAPK, Akt, and NF- $\kappa$ B signaling pathways. *J Agric Food Chem.* 2018;66(3):571–580.
  17. Fang EF, Hou Y, Palikaras K, Adriaanse BA, Kerr JS, Yang B, Lautrup S, Hasan-Olive MM, Caponio D, Dan X, et al. Mitophagy inhibits amyloid-beta and tau pathology and reverses cognitive deficits in models of Alzheimer's disease. *Nat Neurosci.* 2019;22(3):401–412.
  18. Gong Z, Huang J, Xu B, Ou Z, Zhang L, Lin X, Ye X, Kong X, Long D, Sun X, et al. Urolithin A attenuates memory impairment and neuroinflammation in APP/PS1 mice. *J Neuroinflammation.* 2019;16(1):62.
  19. Ballesteros-Álvarez J, Nguyen W, Sivapatham R, Rane A, Andersen JK. Urolithin A reduces amyloid-beta load and improves cognitive deficits uncorrelated with plaque burden in a mouse model of Alzheimer's disease. *Geroscience.* 2023;45(2):1095–1113.
  20. Qiu Z, Zhou B, Jin L, Yu H, Liu L, Liu Y, Qin C, Xie S, Zhu F. In vitro antioxidant and antiproliferative effects of ellagic acid and its colonic metabolite, urolithins, on human bladder cancer T24 cells. *Food Chem Toxicol.* 2013;59:428–437.
  21. Liberal J, Carmo A, Gomes C, Cruz MT, Batista MT. Urolithins impair cell proliferation, arrest the cell cycle and induce apoptosis in UMUC3 bladder cancer cells. *Invest New Drugs.* 2017;35(6):671–681.
  22. Cheng F, Dou J, Zhang Y, Wang X, Wei H, Zhang Z, Cao Y, Wu Z. Urolithin A inhibits epithelial-mesenchymal transition in lung cancer cells via P53-Mdm2-Snail pathway. *Onco Targets Ther.* 2021;14:3199–3208.
  23. Wang Y, Qiu Z, Zhou B, Liu C, Ruan J, Yan Q, Liao J, Zhu F. In vitro antiproliferative and antioxidant effects of urolithin A, the colonic metabolite of ellagic acid, on hepatocellular carcinomas HepG2 cells. *Toxicol In Vitro.* 2015;29(5):1107–1115.
  24. Qiu Z, Zhou J, Zhang C, Cheng Y, Hu J, Zheng G. Antiproliferative effect of urolithin A, the ellagic acid-derived colonic metabolite, on hepatocellular carcinoma HepG2.15 cells by targeting Lin28a/let-7a axis. *Braz J Med Biol Res.* 2018;51(7).
  25. Lv M-Y, Shi C-J, Pan F-F, Shao J, Feng L, Chen G, Ou C, Zhang J-F, Fu W-M. Urolithin B suppresses tumor growth in hepatocellular carcinoma through inducing the inactivation of Wnt/ $\beta$ -catenin signaling. *J Cell Biochem.* 2019;120(10):17273–17282.
  26. Liu F, Cui Y, Yang F, Xu Z, Da L-T, Zhang Y. Inhibition of poly-peptide N-acetyl- $\alpha$ -galactosaminyltransferases is an underlying mechanism of dietary polyphenols preventing colorectal tumorigenesis. *Bioorg Med Chem.* 2019;27(15):3372–3382.
  27. Norden E, Heiss EH. Urolithin A gains in antiproliferative capacity by reducing the glycolytic potential via the p53/TIGAR axis in colon cancer cells. *Carcinogenesis.* 2019;40(1):93–101.
  28. Giménez-Bastida JA, Ávila-Gálvez MÁ, Espín JC, González-Sarriás A. The gut microbiota metabolite urolithin A, but not other relevant urolithins, induces p53-dependent cellular senescence in human colon cancer cells. *Food Chem Toxicol.* 2020;139:111260.
  29. El-Wetidy MS, Ahmad R, Rady I, Helal H, Rady MI, Vaali-Mohammed M-A, Al-Khayal K, Traiki TB, Abdulla M-H. Urolithin A induces cell cycle arrest and apoptosis by inhibiting Bcl-2, increasing p53-p21 proteins and reactive oxygen species production in colorectal cancer cells. *Cell Stress Chaperones.* 2021;26(3):473–493.
  30. Sánchez-González C, Ciudad CJ, Izquierdo-Pulido M, Noé V. Urolithin A causes p21 up-regulation in prostate cancer cells. *Eur J Nutr.* 2016;55(3):1099–1112.
  31. Dahiya NR, Chandrasekaran B, Kolluru V, Ankem M, Damodaran C, Vadhanam MV. A natural molecule, urolithin A, downregulates androgen receptor activation and suppresses growth of prostate cancer. *Mol Carcinog.* 2018;57(10):1332–1341.
  32. Stanisławska IJ, Granica S, Piwowarski JP, Szawka J, Wiązecki K, Czarnocki Z, Kiss AK. The activity of urolithin A and M4 valerolactone, colonic microbiota metabolites of polyphenols, in a prostate cancer in vitro model. *Planta Med.* 2019;85(2):118–125.
  33. Saleem YIM, Albassam H, Selim M. Urolithin A induces prostate cancer cell death in p53-dependent and in p53-independent manner. *Eur J Nutr.* 2020;59(4):1607–1618.
  34. González-Sarriás A, Miguel V, Merino G, Lucas R, Morales JC, Tomás-Barberán F, Alvarez AI, Espín JC. The gut microbiota ellagic acid-derived metabolite urolithin A and its sulfate conjugate are substrates for the drug efflux transporter breast cancer resistance protein (ABCG2/BCRP). *J Agric Food Chem.* 2013;61(18):4352–4359.
  35. Ávila-Gálvez MÁ, Espín JC, González-Sarriás A. Physiological Relevance of the Antiproliferative and estrogenic effects of dietary polyphenol aglycones versus their phase-II metabolites on breast cancer cells: a call of caution. *J Agric Food Chem.* 2018;66(32):8547–8555.
  36. Ávila-Gálvez MÁ, García-Villalba R, Martínez-Díaz F, Ocaña-Castillo B, Monedero-Saiz T, Torrecillas-Sánchez A, Abellán B, González-Sarriás A, Espín JC. Metabolic profiling of



- dietary polyphenols and methylxanthines in normal and malignant mammary tissues from breast cancer patients. *Molecular Nutrition Food Res.* 2019;63(9).
37. Dellafiora L, Milioli M, Falco A, Interlandi M, Mohamed A, Frotscher M, Riccardi B, Puccini P, Rio DD, Galaverna G, et al. A hybrid in silico/in vitro target fishing study to mine novel targets of urolithin A and B: a step towards a better comprehension of their estrogenicity. *Mol Nutr Food Res.* 2020;64(16):e2000289.
38. Totiger TM, Srinivasan S, Jala VR, Lamichhane P, Dosch AR, Gaidarski AA, Joshi C, Rangappa S, Castellanos J, Vemula PK, et al. Urolithin A, a novel natural compound to target PI3K/AKT/mTOR pathway in pancreatic cancer. *Mol Cancer Ther.* 2019;18(2):301–311.
39. Zhang W, Chen JH, Aguilera-Barrantes I, Shiau CW, Sheng X, Wang LS, Stoner GD, Huang YW. Urolithin A suppresses the proliferation of endometrial cancer cells by mediating estrogen receptor-alpha-dependent gene expression. *Mol Nutr Food Res.* 2016;60(11):2387–2395.
40. Huang Y-W, Chen J-H, Rader JS, Aguilera-Barrantes I, Wang L-S. Preventive effects by black raspberries of endometrial carcinoma initiation and promotion induced by a high-fat diet. *Mol Nutr Food Res.* 2019;63(12):e1900013.
41. Alauddin M, Okumura T, Rajaxavier J, Khozoei S, Pöschel S, Takeda S, Singh Y, Brucker SY, Wallwiener D, Koch A, et al. Gut bacterial metabolite urolithin a decreases actin polymerization and migration in cancer cells. *Mol Nutr Food Res.* 2020;64(7):e1900390.